Head and Neck Cancer

28

Inmaculada Rodríguez Jiménez,
María Nieves Cabrera Martín, Antonio Luna,
and José Luis Carreras Delgado

Contents

Abbreviations

^{18}F-FDG	^{18}-fluoro-2-deoxy-D-glucose
ADC	Apparent diffusion coefficient
ASL	Arterial spin labeling
BF	Blood flow
BOLD	Blood oxygen level-dependent
BV	Blood volume
CDI	Conventional diagnostic imaging
CI	Confidence interval
CP	Capillary permeability
CT	Computed tomography
D	Diffusion coefficient
DCE-MRI	Dynamic contrast-enhanced MRI
DCT	Diagnostic computed tomography
DTI	Diffusion tensor imaging
DWI	Diffusion-weighted imaging
EPI	Echo planar imaging
FDA	Food and Drug Administration
FeO_3	nanometer-sized iron oxide
FNAC	Fine needle aspiration cytology
HN	Head and neck
HNSCC	Head and neck squamous cell carcinomas
HPV	Human papillomavirus
IVIM	Intravoxel incoherent motion MR imaging
K^{trans}	Efflux constant
MDCT	Multidetector spiral CT
MRI	Magnetic resonance imaging
MRS	Proton MR spectroscopy

I. Rodríguez Jiménez, MD (✉)
Neuroradiology, RESSALTA, Health Time Group,
San Juan de Dios and Cruz Roja Hospitals,
Córdoba, Spain
e-mail: i.rodriguez.o@htime.org

M.N. Cabrera Martín, MD
Department of Nuclear Medicine,
Clínico San Carlos Hospital, Madrid, Spain
e-mail: mncabreram@hotmail.com

A. Luna, MD
Chief of MRI, Health Time Group, Jaén, Spain

Department of Radiology, University Hospitals,
Case Western Reserve University,
Cleveland, Ohio, USA
e-mail: aluna70@htime.org

J.L. Carreras Delgado, MD, PhD
Department of Nuclear Medicine,
Clínico San Carlos Hospital, Madrid, Spain
e-mail: jcarreras.hcsc@salud.madrid.org

A. Luna et al. (eds.), *Functional Imaging in Oncology*,
DOI 10.1007/978-3-642-40582-2_5,

MTT	Mean transit time
MTV	Metabolic tumor volume
PET	Possitron emision tomography
PET/CT	Possitron emision tomography/ computed tomography
PP	Perfusion-related parameter
SCC	Squamous cell carcinoma
SUV	Standardized uptake values
TLG	Total lesion glycolysis
USPIO	Ultrasmall particulate iron oxide

28.1 Introduction

By far, squamous cell carcinoma (SCC) is the most common neoplasm in the head and neck (HN), corresponding to 90 % of all cancers in this region and to 5 % of all cancers. Other neoplasms of HN are most likely to involve the lymph nodes, including secondary involvement in metastatic lesion and lymphoma. Risk factors for head and neck squamous cell carcinomas (HNSCC) can include tobacco and human papillomavirus (HPV). The status of the cervical lymph nodes is one of the most important prognostic factors of this tumor. When nodal metastases exist, cure rates decrease by approximately 50 % [1]. Computed tomography (CT) and magnetic resonance imaging (MRI) are noninvasive techniques routinely performed for tumor characterization, local and nodal staging, monitoring response, assessment of therapeutic response and recurrence detection [2, 3]. Management decisions have to be based on the involvement of adjacent structures, beyond the primary tumor site and the presence of perineural or perivascular spread.

Imaging studies can detect metastatic adenopathies better than clinical examination, especially in not accessible locations, such as retropharyngeal and paratracheal regions. Imaging also plays an important role in monitoring tumor response and in detecting recurrent or persistent disease, sometimes before it is clinical evident.

Lymphoma is the second most common malignancy in HN, including Hodgkin disease and non-Hodgkin lymphoma. Typical features are focal or diffuse enlargement of lymph nodes, which are usually well-demarcated and homogeneous with remarkable enhancement. Extranodal extension, necrosis, calcification, or hemorrhage are rare features in non-treated patients, and these findings could be useful to distinguish lymphoma from lymph node metastasis.

Metastases from aerodigestive superior tract tumors or glandular, salivary, or thyroid malignancies, especially papillary carcinoma, are infrequent causes of cervical lymphadenopathy. Moreover, lymphadenopathy can be the first clinical manifestation in some of them. Differential diagnosis of cervical lymphadenopathy includes infection, granulomatous, or inflammatory conditions.

28.2 Imaging Techniques in the Assessment of Head and Neck Neoplasms

28.2.1 Morphological Imaging Modalities

28.2.1.1 Ultrasonography

Different imaging techniques are available to assess HN neoplasms. Ultrasonography associated with fine needle aspiration cytology (FNAC) is a widely used technique for nodal characterization due to its low cost and accessibility. However, in a multicenter study, the combination of ultrasound-guided FNAC had no significant additional value over other noninvasive imaging modalities in the assessment of neck node metastases [4, 5]. On the other hand, there are some advantages of this technique in the evaluation of superficial structures, such as thyroid [6] and salivary glands [7]. These advantages could be listed as the high spatial resolution, the low cost of this technique and the absence of ionizing radiation.

28.2.1.2 Computed Tomography (CT) and Magnetic Resonance Imaging (MRI)

A more advanced imaging modality, like CT and MRI, is mandatory to be performed in the pretherapeutic staging or treatment monitoring in patients with HN tumors. With wider availability, relatively low cost and shorter examination time, CT is more extensively used in clinical practice. Nevertheless, it has a relative low soft tissue contrast resolution compared to MRI [8, 9]. Nowadays, multidetector spiral CT (MDCT) reduces partial volume averaging, acquisition time, and motion artifacts. Another advantage of MDCT is the capability of multiplanar

reconstruction and 3D imaging, especially useful for osseous evaluation and virtual endoscopy of the larynx, hypopharynx, or trachea. This technique shows high sensitivity in the identification of exophytic lesions in these areas. MRI can improve visualization and characterization of some tumors, due to its higher contrast resolution, and it is preferred in the assessment of uncommon malignancies or nasopharyngeal, salivary gland, or sinusal lesions. It can also be used as a complementary tool to detect cartilage invasion in laryngeal tumors, neural infiltration, or nodal metastases [10, 11]. However, in the postreatment setting, in order to increase the diagnostic yield in the differentiation of small recurrences from vascularized scar tissue or in the detection of preclinical recurrences, it is necessary to integrate morphological CT or MRI with other functional approaches, recently incorporated in daily clinical practice. Recent reports have demonstrated the utility of functional data associated to conventional imaging techniques in the assessment of HN lesions, allowing a more accurate evaluation than using only a purely morphological imaging modality.

28.2.2 Functional Imaging Techniques

28.2.2.1 Perfusion and Permeability

Until very recently, one of the most important limitations of perfusion CT was the restriction of the coverage area. Thus, the estimation of perfusion parameters was usually restricted to small volumes. In addition, this limited coverage could not permit the estimation of perfusion parameters of both the primary tumor and associated nodal involvement in all patients. Another consideration in patients submitted to repetitive CT studies for monitoring treatment effects was the increased exposure to radiation that is higher for perfusion studies than for standard CT studies [12, 13].

The possibility of more extensive coverage, the integration with other advanced sequences, and the ability of fast dynamic studies without the use of ionizing radiation have contributed to a wide development of MRI perfusion techniques. In spite of the possibility to combine information from standard CT and MRI techniques, the identification of small nodal metastasis, and also the distinction of post-therapeutic tissue changes from residual tumor remain challenging for morphological imaging approaches. Therefore, several functional techniques, especially MRI-derived ones, have been rapidly developed in recent years. The most extended MRI applications are dynamic contrast-enhanced MRI (DCE-MRI) and diffusion-weighted imaging (DWI) [14]. Deconvolution-based perfusion MRI and CT studies can help assessing physiologic parameters related with tumor growth or angiogenesis, such as blood flow (BF), blood volume (BV), mean transit time (MTT), or capillary permeability (CP). Angiogenesis determines increased perfusion, BV, and CP according to the degree of neovascularization associated with the tumor [15]. This implies that perfusion CT of the HN would be a useful tool in differentiating malignant tumors from other processes. Some authors found direct correlation between tumor angiogenesis measured by perfusion CT studies and histological grade and T stage [16, 17]. Another advantage of these techniques is the potential ability to predict treatment response. For instance, tumor hypoxia in HN cancers is associated to worse response to radiotherapy and chemotherapy, while tumors that show increased BV and BF are better responders to adjuvant treatments.

The main advantage of DCE-MRI is the possibility to evaluate the angiogenesis of the primary tumor and to establish an accurate locoregional nodal stage in a single study. DCE-MRI is also considered a useful tool in assessing hemodynamics with higher resolution and specificity. Different characteristics in perfusion MRI of the primary tumor and metastatic nodes do not allow an extrapolation of results obtained from primary tumors to regional disease. Advanced disease is determined by T and N stages, and locoregional analysis seems to be better assessed by new functional techniques, such as perfusion-weighted MRI or PET/CT [18]. Nowadays, DCE-MRI studies are usually performed using fast GE T1-weighted sequences (DCE-MRI) or more exceptionally by means of T2-weighted techniques (dynamic susceptibility contrast MRI). To increase the signal contrast between tumor and the normal adjacent tissue, fat-suppressed T1-weighted images are preferred in the HN area for perfusion MRI. The signal intensity curve morphology allows differentiating benign and malignant tissues in clinical

practice. Quantitative parameters from perfusion studies can be obtained in a simple approach using curve descriptor like contrast arrival time (time when the contrast arrive to a pixel), time to peak (time for the maximum signal intensity), or area under the curve (AUC, integral of the contrast concentration time curve for a specific time interval definition). One step further is the use of pharmacokinetic modeling, which permits the calculation of parameters that depend on tumor blood flow and microvascular permeability. Derived parameters of this analysis, such as K^{trans}, that depends on tumor blood flow and microvascular permeability, has been related to better follow-up prediction. The calculation of pretreatment K^{trans} and the evaluation of its changes with treatment may be a useful prognostic marker in HN tumors [18, 19].

In patients with renal insufficiency or difficulties for administration of intravenous contrast, arterial spin labeling (ASL) could be used, as this technique does not require the administration of a contrast agent. ASL is a MRI technique that offers information similar to that provided by conventional dynamic susceptibility sequences. ASL has been used to evaluate oncologic patients treated with anti-angiogenic or vasomodulator agents. The application of this approach is based on the monitoring of the changes in tumor oxygen supply. Therefore, it is a potential useful method to measure response to treatment of HN tumors without the need of exogenous contrast agent [20–22].

It is important to consider the presence of regional nodal infiltration, because the malignant involvement of a single node is related to a reduction of the disease-free survival in about 50 %. If bilateral nodal affectation exists, the survival is even more reduced. Consequently, the characterization of nodal metastases is of prime importance for therapeutic decisions, strategies, and outcome. Some reports aim to determine the prognostic value of DCE-MRI in the assessment of malignant HN lymphadenopathies and its ability to predict patients' survival (Fig. 28.1). In addition, DCE-MRI has a promising role in the assessment of tumor capability for causing metastatic dissemination and treatment resistance in a noninvasive approach. A recent publication described that this technique could be useful to assess the increased interstitial fluid pressure that force fluid from the microvasculature to interstitium, causing interstitial hypertension, as this process is related to metastatic dissemination and treatment resistance [23]. Another attractive role of DCE-MRI is the assessment of tumor perfusion associated to PET studies. The fusion of MRI and PET images or the use of hybrid integrated PET-MRI equipment provides several potential advantages compared with CT as morphological guide for PET in HN region, such as a better soft tissue contrast and less susceptibility to artifact from dental implants, which may be especially useful in the evaluation of potential metastatic lymphadenopathies and local recurrence of tumors [24].

28.2.2.2 Diffusion-Weighed Imaging (DWI) and Diffusion Tensor Imaging (DTI)

Diffusion-weighted imaging (DWI) has been extensively used outside the brain in recent years, due to its ability in evaluating the rate of water diffusion in different tissues. This technique may be quantified by means of apparent diffusion coefficient (ADC), which has been used in the HN region for tumor characterization, as ADC tends to be lower in malignant tumors than in normal tissues or benign lesions, secondary to its hypercellularity [25–27].

Most commonly, echo-planar-imaging (EPI) sequences are used in the HN region. The challenge is to ensure good quality acquisitions, as EPI sequences are prone to distorsion and susceptibility artifacts, which are frequent in HN region due to air-soft tissue-bone interfaces, involuntary or deglutition motions (breathing or swallowing), physiologic vascular pulsation and dental fillings with metallic materials. Therefore, it is interesting to reduce scanning time to no longer than 5 minutes. The use of parallel imaging or advanced strategies, such as periodically rotated overlapping parallel lines with enhanced reconstruction (PROPELLER), make this objective possible. In some difficult cases, turbo spin-echo-based sequence can be used instead of EPI sequence [25, 27]. In order to perform ADC quantification, it is necessary to obtain at least two b values. More commonly a low b value between 0 and 100 s/mm^2, and a high b value between 800–1,000 s/mm^2 are obtained. The inclusion of low b values under 300 s/mm^2 could overestimate ADC measurements for the combination of perfusion and

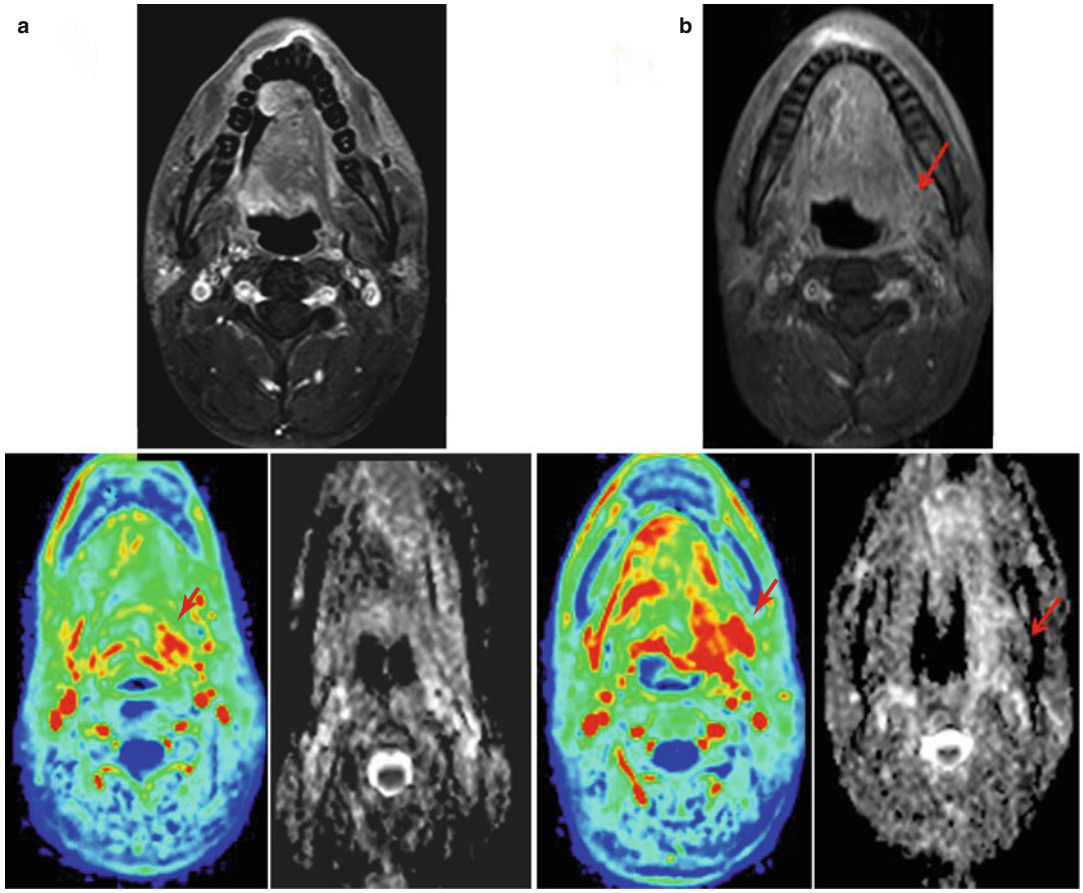

Fig. 28.1 Recurrence and postreatment progression of treated oropharynx cancer. (**a**) Suspected tumor recurrence was not well identified on postcontrast TSE T1-weighted image (*a*, *top image*) and ADC map (*a*, *right bottom image*). However, perfusion parametric map (*a*, *left bottom image*) was able to identify a suspicuous region (*arrow*) and was also useful to guide biopsy, which was positive for malignancy. (**b**) After the first cycle of chemotherapy, postcontrast TSE T1-weighted image (*b*, *top image*) showed an area of irregular enhancement with mass effect on the left oropharyngeal space (*arrow*). Both perfusion and ADC map (*b*, *bottom left* and *right images*, respectively) demonstrated more clearly tumor progression (*arrows*) in a patient that was not responding to treatment

diffusion information. Le Bihan et al. [28] described the capability to distinguish molecular diffusion from perfusion, acquiring multiple b values lower than 100 s/mm^2 and values greater than this threshold using intravoxel incoherent motion (IVIM) model of analysis of diffusion signal decay, that provides perfusion and diffusion information in a single sequence. Calculation and quantification of IVIM-derived parameters, such as D* (perfusion contribution to signal decay), D (real diffusion of water molecules) and *f* (perfusion contribution to the diffusion signal) are being tested for the evaluation of several diseases and organs. These parameters are different among various types of HN tumors. The application of the IVIM model in the HN area has been studied by some authors and its clinical role is not well defined yet [25, 29, 30] (Fig. 28.2).

ADC has shown a role in the differentiation between benign and malignant tumors in HN region, different thresholds have been proposed for this task (range 1.22–1.30 × 10–3 mm^2/s). However, even more different values of the ADC have been used for characterization of tumor type. The most frequent tumor in the HN area, SCC, usually shows an intermediate grade of malignancy, while other tumors present a higher cellular density and lower ADC values such as malignant lymphomas (Fig. 28.3). Some authors propose the distinction of subtypes of SCC and different histopathological subtypes of lymphomas according to ADC values. Non-Hodgkin lymphomas demostrate lower ADC

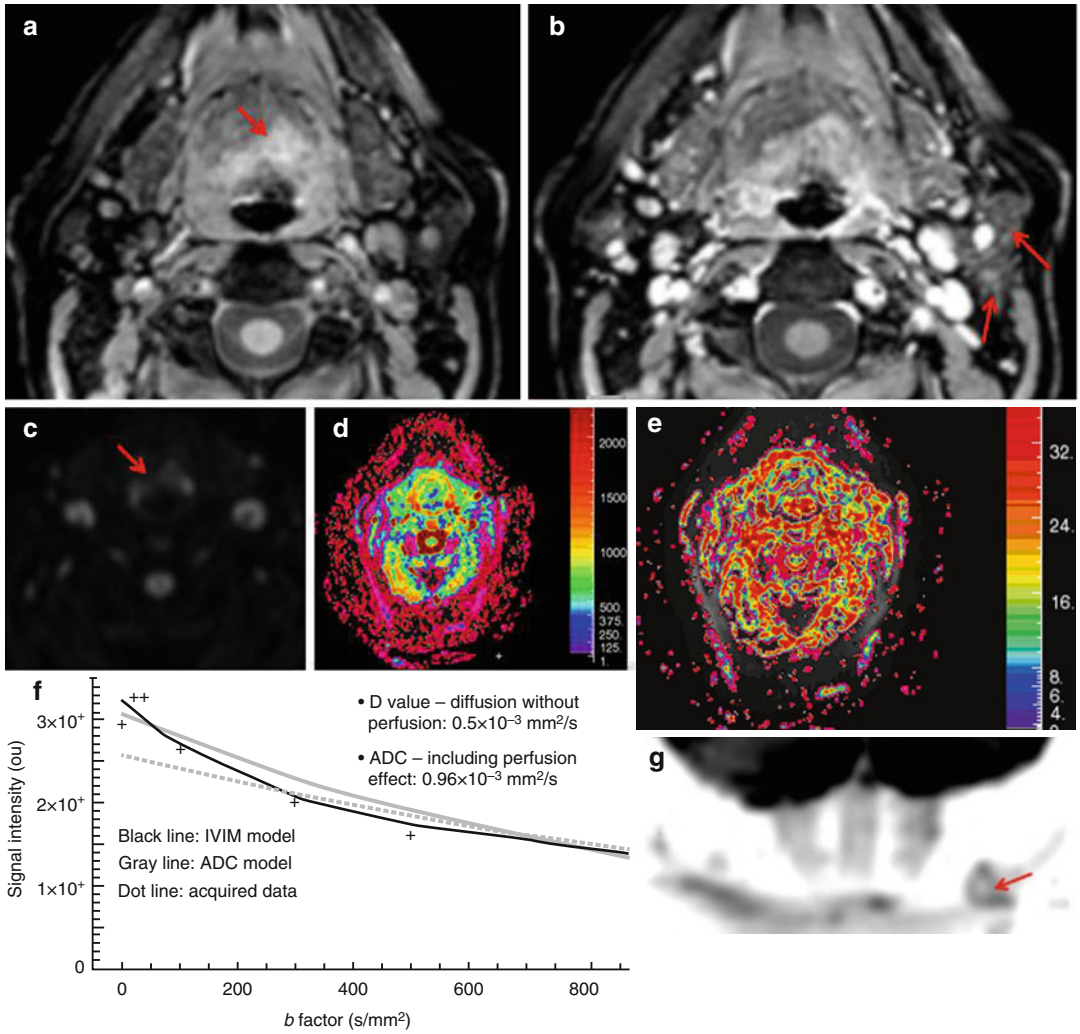

Fig. 28.2 Supraglottic oropharynx cancer with ipsilateral nodal metastasis (T3N1b stage). (**a**, **b**) Postcontrast THRIVE images show an enhancing expansive lesion at the left supraglottic space (*arrow*, **a**) that extended both to hypopharynx and left pyriform sinus, with involvement of ipsilateral lymph nodes (*arrows*, **b**). (**c**) DWI with a b value of 1,000 s/mm better depicts the mass as it shows restriction of diffusion consistent with malignancy (*red arrow*). (**d**, **e**) A biexponential model of analysis of the diffusion signal decay was used to obtain parametric maps of *D* (diffusion without perfusion contamination) and perfusion fraction, respectively. (**f**) The diffusion signal decay of the mass is shown in the graph (x-axis represents the *b* values and y-axis the signal intensity). Notice the great difference between ADC (0.96×10^{-3} mm^2/s) and D (0.5×10^{-3} mm^2/s) values due to the effect of the mass perfusion. The perfusion fraction of the mass was high (35 %), and it was estimated using only the diffusion signal decay for *b* values lower than 100 s/mm^2. (**g**) Coronal MIP of DWIBS sequence with inverted gray scale demonstrates the restriction of free water motion of left lymphadenopathy (*arrow*)

values than Hodgkin lymphoma. However, there are still some limitations in the utility of DWI to differentiate poorly differentiated SCC from lymphomas and necrotic tumors from infections with necrotic areas [25, 27, 28, 31–38].

The application of DWI is useful for the characterization of salivary gland tumors. It has been shown useful in the distinction between pleomorphic adenoma, which shows high ADC values, from Warthin tumors, with lymphoid origin, and other heterogeneous tumors and carcinomas. Furthermore, some authors have also proposed that the use of DWI could avoid biopsies in cases of pleomorphic adenomas [39]. Another important clinical application of this technique is the evaluation of lymph nodes, because malignant

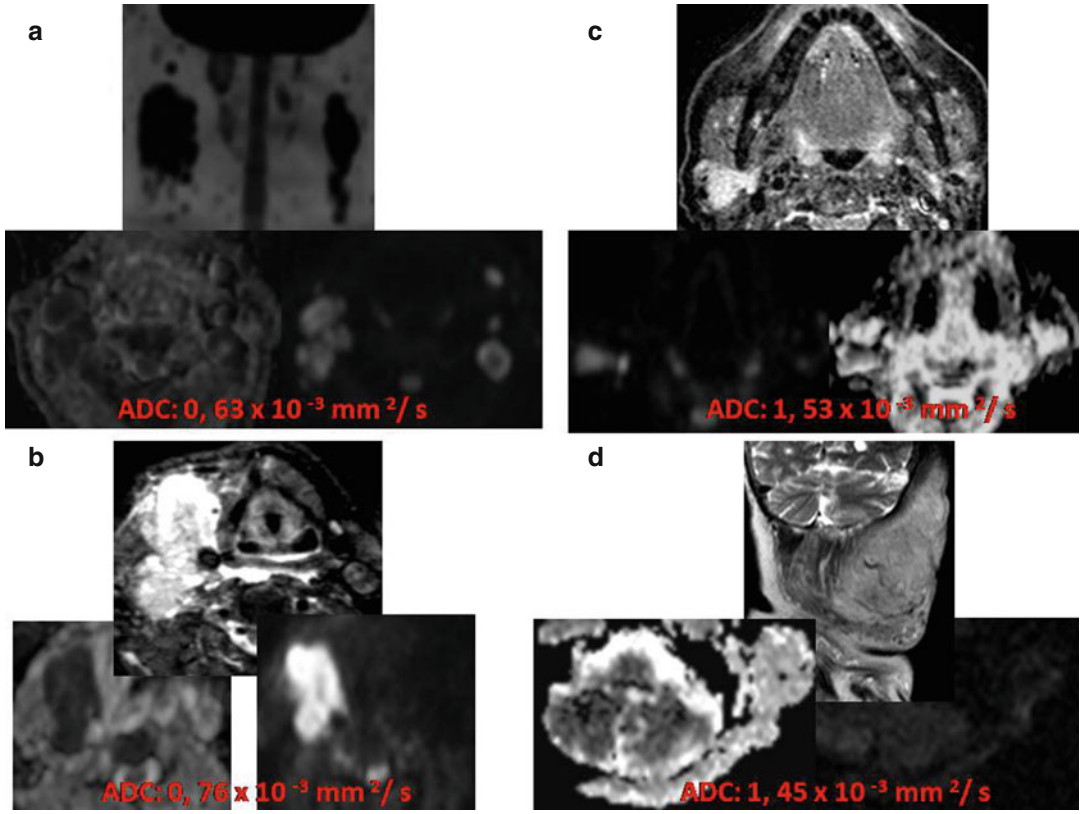

Fig. 28.3 Differences in ADC value can be considered for determining the chance of malignancy of an HN lesion. (**a**) Extensive bilateral lymphadenopathies in HN region demonstrating high signal on high *b* value and low ADC values due to lymphoma. (**b**) Undifferentiated occult carcinoma with right lymphadenopathy presenting also high signal on high *b* value and low ADC, but higher than lymphoma. Two benign lesions: a right pleomorphic adenoma (**c**) and a left plexiform neurofibroma (**d**); both benign lesions have higher ADC values very different from the low values observed in malignant lesions

lymphadenopathies show significant lower values than benign or reactive nodes. Despite the high sensitivity and specificity of DWI, PET/CT is the method of choice to determine cervical node involvement. The limitation of DWI in the evaluation of lymph node includes small size of some cervical malignant lymph nodes and the presence of some inflammatory, granulomatous, or infectious diseases that presents with reactive nodes, which could be associated with high cellular density, homogeneous and intense lymphoid infiltration, or fibrous stroma, descending all of these factors ADC measurements of lymph nodes (Fig. 28.4). The presence of necrosis in lymphadenopathy could make its adequate characterization difficult, because ADC values can increase. For that reason, it is recommended to exclude necrotic areas from ADC measurements [25, 27, 31, 33–36, 38, 39].

Another particular use of DWI is the characterization of cystic lesions in children. During childhood, there is a high incidence of congenital lesions and cysts. These lesions should be distinguished from malignant tumors, which are often very aggressive at these ages. Cystic lesions of HN can be routinely diagnosed with conventional MRI sequences, but in certain situations such as infected branchial cleft cysts or epidermal cysts, DWI can play an important complementary role. Epidermal cysts are typically associated with restricted diffusion and low ADC values due to their keratinous content. These lesions are frequently found in HN region during the first decade of life. Fewer differences in ADC values among cystic lesions are caused by protein component variations in the fluid and the changes in the viscosity of the contents [31, 40].

Another advanced technique derived from DWI, diffusion tensor imaging – DTI – may be

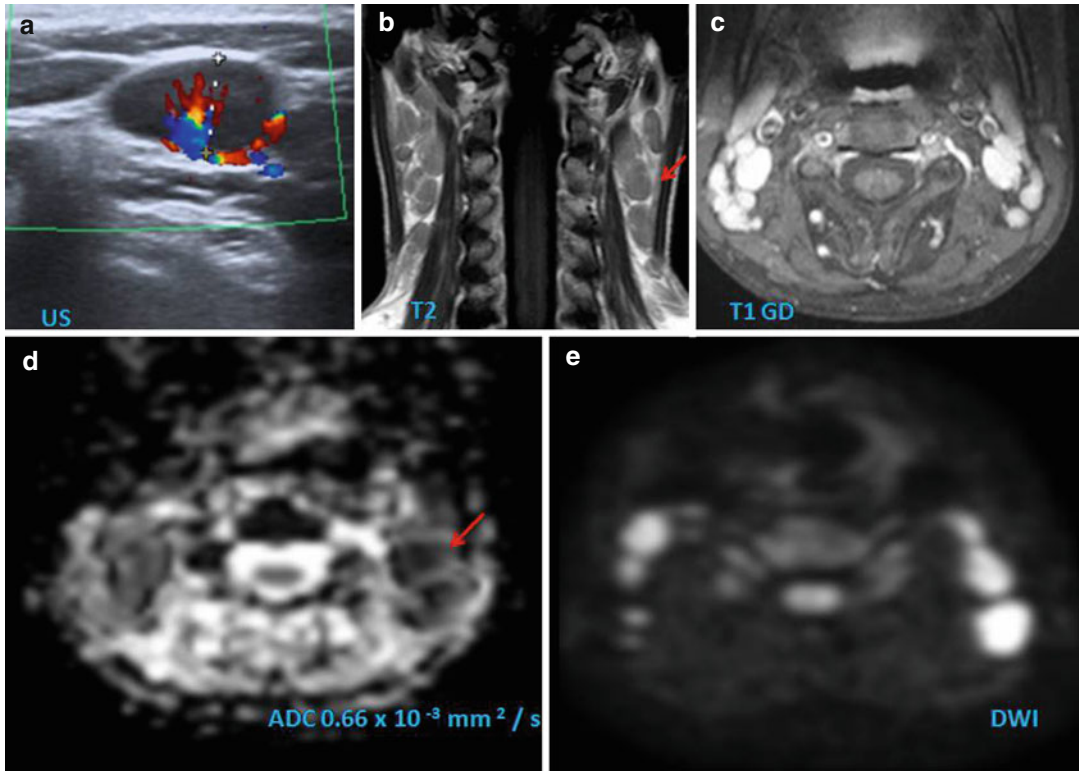

Fig. 28.4 This case can be considered a pitfall of morphological imaging. This child presents multiple bilateral lymphadenopathies, which are hypoechoic and show hilar hypervascularization on Doppler ultrasound (**a**). The lymph nodes present low to isosignal intensity to muscle on T2-weighted image (*arrow*, **b**) and an intense and homogenous enhancement on fat-suppressed TSE T1-weighted sequence after administration of contrast agent (**c**). On DWI, the nodes demonstrate restricted diffusion, demonstrated as low measurement of ADC values (*arrow*, **d**) and high signal on high *b* value (**e**). Although these findings can be also found in malignant lymphadenopathies or lymphoma, the clinical history and histological analysis confirm the diagnosis of Still's disease

useful in surgical planning in patients with HN mass lesions, providing information about the localization of nerve bundles and their relation with the mass, helping the surgeons to preserve these fibers and prevent them to be removed [41].

28.2.2.3 MR Spectroscopy

Another advanced technique associated to MRI is proton MR spectroscopy (MRS). This technique has the ability to detect specific metabolites in the analyzed tissues. Despite the difficulties to obtain good-quality MRS spectra in HN region, some studies have demonstrated elevated Cho/Cr ratios in HN malignant tumors compared with normal tissues. Other cervical lesions with cellular proliferation, such as glomus tumors, schwannomas, and inverted papillomas, also show increased Cho/Cr ratios [42, 43]. Although, the main potential clinical application of proton MRS is therapy monitoring in patients with HN cancer, its use is very limited due to technical difficulties to be applied in a clinical setting.

28.2.2.4 Blood Oxygen Level-Dependent (BOLD) Technique

Hypoxia is a pivotal factor ot the pathophysionome of HN cancer, since it can promote tumor progression and resistance to therapy. BOLD MRI may provide a noninvasive assessment of tumor hypoxia by monitoring changes in solid tumor concentration. BOLD is capable to distinguish a focal increase in blood flow, by the detection of changes of local T2* signal, secondary to a decrease of oxyhemoglobin and increase of deoxyhemoglobin contents. This process is known as BOLD effect. BOLD is able to detect differences in tissue oxygenation using physiologic and pharmacologic challenges such as

hyperoxia, hypoxia or hypercapnia. The measurement of tumor oxygenation using BOLD studies can be correlated with tumor microvasculature. In patients with primary HN tumors, positive nodal status was correlated with a widened oxygenation distribution in the tumors [44]. However, BOLD MRI is still far from the clinical arena.

28.2.2.5 New Contrast Media

Other MRI contrast agents than gadolinim chelates have been investigated specially for assessment of nodal status. Typically they are composed of nanometer-sized iron oxide (FeO_3) particles coated with dextran or ultrasmall particulate iron oxide (USPIO). These agents are phagocytized by macrophages, and they are especially used in the study of the lymph nodes. Tumor lymphadenopathies show a pattern of reduced contrast uptake, while nodes with benign hyperplasia have a normal contrast enhancement. These agents are not sensitive for detecting micrometastases. SPIO-enhanced MRI is emerging as an important tool for planning the extent of surgery, although its clinical use is still limited due to lack of FDA approval [45].

28.2.3 Molecular Imaging

Sensitivity of PET in detecting primary tumors is similar to that of the conventional diagnostic imaging (CDI) with the exception of tumors located in the oral cavity, with a sensitivity up to 98 % [46, 47]. A limitation of PET is its inability to define the depth of invasion and the relation to neighboring structures. Clinical examination and structural imaging can compensate this deficiency. In the current era of multimodality imaging devices, many groups, including our own, are performing diagnostic computed tomography (DCT) with intravenous contrast as part of the PET/CT acquisition protocol. In the study by Veit-Haibach et al., PET/DCT was superior in TNM staging of HN cancer compared to contrast-enhanced CT only and PET/CT [48]. This was based on a more reliable T staging, partly due to better primary tumor delineation on co-registered PET/DCT in patients with metallic artifacts. PET/DCT could lead to a change in patient management in a substantial number of patients when compared to CT and PET/CT. Moreover, PET/CT is able to detect an unknown primary tumor, in situations where there is a strong clinical suspicion of a primary tumor despite a negative biopsy and in cases where more extensive disease can be demonstrated than could be observed on clinical examination or on other imaging techniques [49] (Fig. 28.5).

PET/MRI has the potential to improve diagnostic imaging in patients in whom the soft tissue contrast provided by CT is considered insufficient. Further studies are needed to evaluate the clinical role of PET/MRI in HN cancer [50]. CDI requires an alteration in the size or architecture of nodes for disease detection [51]. This is not a requirement for PET positivity. In a review published by Schöder et al., the utility of PET and CT in assessing cervical lymph nodes in patients with HNSCC was compared [52]. PET was found to have a higher sensitivity and specificity compared with MRI or CT in the detection of cervical nodal disease in HNSCC (sensitivity 87–90 % versus 80–93 %, specificity 80–93 % versus 21–100 %) [46]. Similar findings were achieved in the study performed by Iyer et al. [53]. Murakami et al., according to receiver operating characteristic (ROC) analysis, established that the size-based SUV_{max} cutoff values were 1.9, 2.5, and 3.0 for lymph nodes <10 mm, 10–15 mm, and >15 mm, respectively [54]. These cutoff values yielded 79 % sensitivity and 99 % specificity for nodal-level staging. Jeong et al. prospectively compared PET and PET/CT in assessing cervical nodal status in HN cancer patients [55]. PET/CT provided additional information for anatomic localization with regard to metastatic lymph node level and a correct differentiation between malignant nodes and benign lesions leading to a change in extent of neck dissection in 10.6 % of patients. Addition of CT fusion led to a 15 % increase in accuracy of nodal staging compared with PET alone. In a meta-analysis including 32 studies (1,236 patients), ^{18}F-FDG-PET sensitivity was 79 % (95 % CI = 72–85 %) and specificity was 86 % (95 % CI = 83–89 %) [56]. For cN0 patients, sensitivity of ^{18}F-FDG-PET was only 50 % (95 % CI = 37–63 %), whereas specificity was 87 % (95 % CI = 76–93 %). In studies in which both ^{18}F-FDG-PET and CDI were performed, sensitivity and specificity of ^{18}F-FDG-PET were 80 and 86 %, and sensitivity and specificity of CDI were 75 and 79 %, respectively. PET/DCT

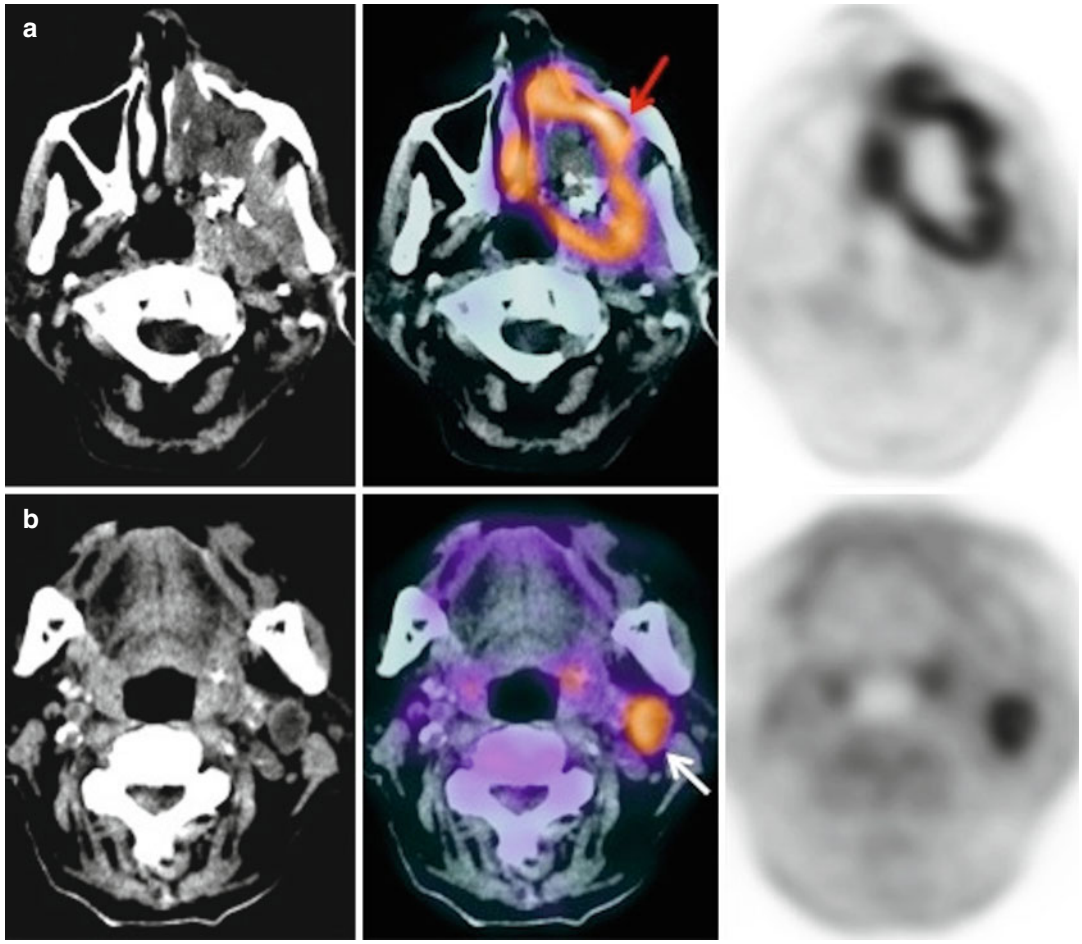

Fig. 28.5 An 80-year-old woman with fever and constitutional syndrome. The patient was treated with antibiotics for suspected left maxillary sinusitis, without symptom improvement. With the suspicion of a malignant disease, a ^{18}F-FDG-PET/CT study was requested. Extensive lesion was observed in left maxillary sinus (**a**, *red arrow*) and ipsilateral cervical adenopathy (**b**, *white arrow*). The biopsy of the adenopathy confirmed a squamous cell carcinoma of the maxillary sinus with lymph node involvement

demonstrates a significantly better performance than both contrast-enhanced CT and PET/CT protocols in detecting nodal metastases, especially in the depiction of small (<15 mm) nodal metastases. Rodrigues et al. demonstrated a fourfold increase in nodal detection [57] (Fig. 28.6).

Recently, Prestwich et al. assessed the utility of ^{18}F-FDG-PET/CT as an adjunct to CDI in patients with locally advanced HNSCC [58, 59]. The N stage was changed in 40 % of cases. In conclusion, although PET/CT has a higher diagnostic accuracy and specificity than CDI for evaluation of lymph nodes (N stage), its information is not reliable enough to avoid lymphadenectomy in negative cases [60]. Several studies have estimated sensibility of PET/CT in the detection of distant metastases. In a prospective study, PET/CT detected additional metastases in 6 % of patients, compared with thoracic CT [61]. Ng et al. compared PET and body CT for M staging. Sensitivity for PET and CT were 76.9 and 50 %, respectively, with impact on treatment in 13.1 % of cases [62]. Lonneaux et al. published their experience in the use of PET or PET/CT in the staging of patients with HNSCC [63]. All patients had CT or MRI imaging of the HN region and thoracic CT with discordant TMM stages in 43 % of patients. In cases of discrepancy, ^{18}F-FDG-PET showed better accuracy and changed treatment in 13.7 %. The change in M stage occurred in 8.6 % of cases. The most common locations of distant metastasis were the lungs, followed by bone (Fig. 28.7) and liver.

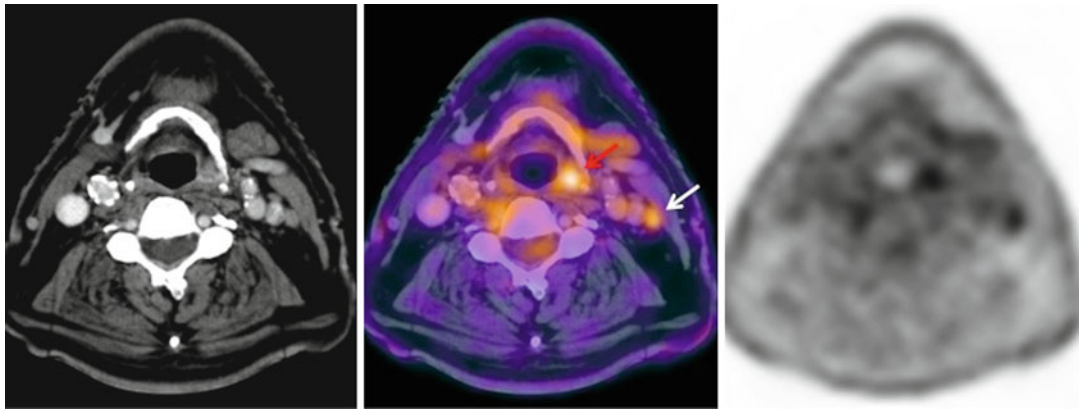

Fig. 28.6 A 78-year-old man with hypopharynx squamous cell carcinoma, T2N0M0 in CT. ^{18}F-FDG-PET/CT showed intense uptake in the lesion in the left pyriform sinus (*red arrow*) and in an ipsilateral millimeter-sized lymph node (*white arrow*). FNA of the lymph node confirmed metastatic disease

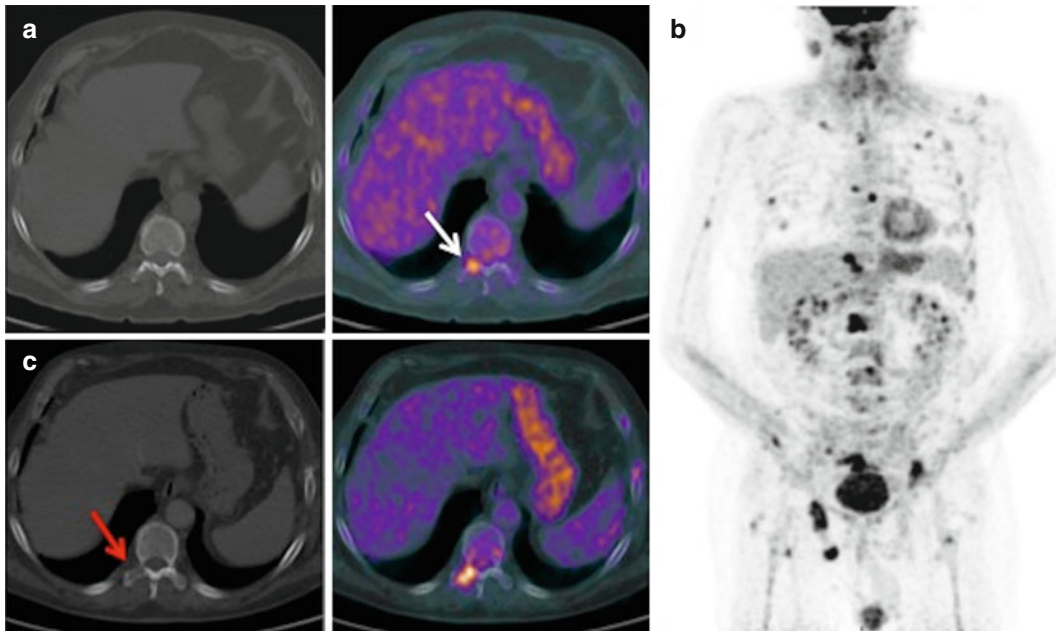

Fig. 28.7 A 68-year-old man with right pyriform sinus carcinoma treated with laryngeal microsurgery, chemotherapy, and radiotherapy. In the staging ^{18}F-FDG-PET/CT, pathologic FDG uptake was observed in D11 (**a**, *white arrow*) and L1 vertebral bodies, without CT correlation. In post-chemotherapy ^{18}F-FDG-PET/CT (**b**), bone progression of the known vertebral metastasis and multiple new lesions were observed. With disease progression, the lesion of T11 vertebral body was apparent on CT as a lytic area (**c**, *red arrow*)

28.3 Treatment Response

The early treatment response assessment using PET/CT has been analyzed in few studies, some of which show a correlation between the decrease in ^{18}F-FDG uptake and improved locoregional control. There are insufficient data on the use of PET/CT in the assessment of induction chemotherapy. It aims to optimize the most appropriate treatment for each patient after neoadjuvant therapy, selecting the responder patients that could benefit from concurrent chemoradiotherapy. Nonresponder patients would be candidates for more aggressive surgery after induction [64].

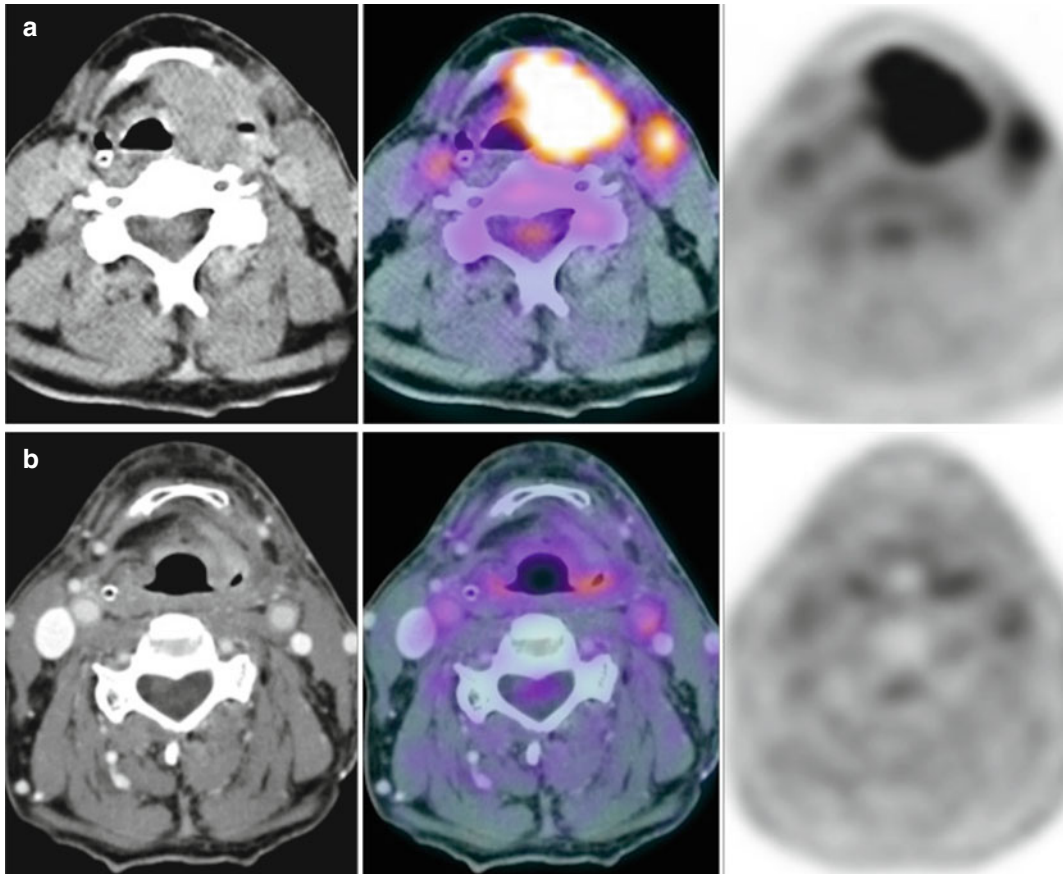

Fig. 28.8 A 70-year-old man with squamous cell carcinoma of the larynx T3N2bM0 was clearly depicted with ^{18}F-FDG-PET/CT (**a**) performed before chemoradiation. ^{18}F-FDG-PET/CT scan at 10 weeks after the completion of treatment (**b**) showed complete response which was confirmed after laryngeal microsurgery with biopsy and left functional neck dissection

Response rates at the site of primary disease are generally high with concurrent chemoradiotherapy. Therefore, the aim of post-therapy PET/CT is the detection of residual disease in neck lymph nodes. Most studies on post-therapy ^{18}F-FDG-PET in HNSCC included heterogeneous patient populations, and all the data come from retrospective analyses. Selection criteria were different: patient selection, disease sites, treatment strategies, treatment protocols, time for PET in response assessment, and the use of PET/CT versus PET. Only a few recent studies analyze the role of combined PET/CT in this setting [65]. Most authors state that posttreatment PET should not be performed before 10–12 weeks after the end of therapy. At this time, most inflammatory changes have decreased, and therefore, the possibility of false-positive results is lower [66]. The true value of post-therapy ^{18}F-FDG-PET in patients treated with radiotherapy or chemoradiotherapy is the high negative predictive value [58, 59, 67–69] (Fig. 28.8). Many patients who might otherwise proceed to biopsy or neck dissection can be observed with clinical follow-up and periodic imaging studies. However, it would be advisable to perform prospective studies with similar selection criteria, to establish the true accuracy of PET/CT in this indication [66]. A recent cost-effectiveness analysis supports the use of PET/CT as the more cost-effective strategy for surveillance of neck after completion of definitive chemoradiotherapy compared to up-front neck dissection in N2 disease [70]. There is a growing trend to consider tumor metabolic information when planning treatment and predicting outcome. Metabolic tumor volume (MTV) is determined either using a fixed background SUV cutoff, all voxels containing SUV values above this threshold constituting the MTV, or using the SUV_{max} values of the individual tumor sites involving the

region growing up to a prefixed percentage of the SUV_{max}. When multiplying MTV by the mean SUV, total lesion glycolysis (TLG) is obtained. This could prove to be another biomarker of potential interest for prognosis assessment in cancer patients. Chung et al. established a cutoff of 40 mL as the best discriminative value for MTV, to predict short-term outcome to radiotherapy or chemoradiotherapy in pharyngeal cancer [71]. Patients with MTV >40 mL showed a significantly lower number of complete response/no recurrence than did patients with MTV ≤40 mL.

In the posttreatment setting, DWI has shown promise in the distinction between benign posttreatment changes and residual or recurrent SCC. Persistent tumor usually shows lower ADC values than postherapeutic fibrosis [33]. Interestingly, these results also occurs in the early postreatment period when PET is limited. The best strategy for therapy monitoring with DWI is to perform consecutive ADC measurements during the course of therapy, as a relative decrease in lesion ADC during treatment is a stronger marker than a single low ADC measurement of the suspicious lesion [33]. In addition, DWI has been proposed to predict response to therapy [27]. Primary tumors with lower ADC values are more likely to have a complete response to chemoradiation. In a similar way, metastatic lymph nodes with low ADC values also generally show better response to treatment.

In addition, the integration of DCE-MRI in MRI protocols has also increased in popularity in this setting. Perfusion measurements can be used as a good parameter for tumor response. Reduction of tumor perfusion parameters just after initiation of radiotherapy can be an early indicator of local control in HN cancer. However, there is no variation in blood volume measurements in patients that demonstrated local resistance to chemoradiation [18, 72].

28.4 Recurrence Detection

The use of advanced functional techniques along with morphological MRI, especially DWI, is important in tumor follow-up due to their ability to differentiate recurrence from iatrogenic changes such as edema or fibrous and inflammatory reactions. Recent studies suggest that an increase in the ADC during treatment could be associated to favorable treatment response; meanwhile, minimal increase or decrease in ADC values suggests a treatment failure (Fig. 28.9). In addition, DWI

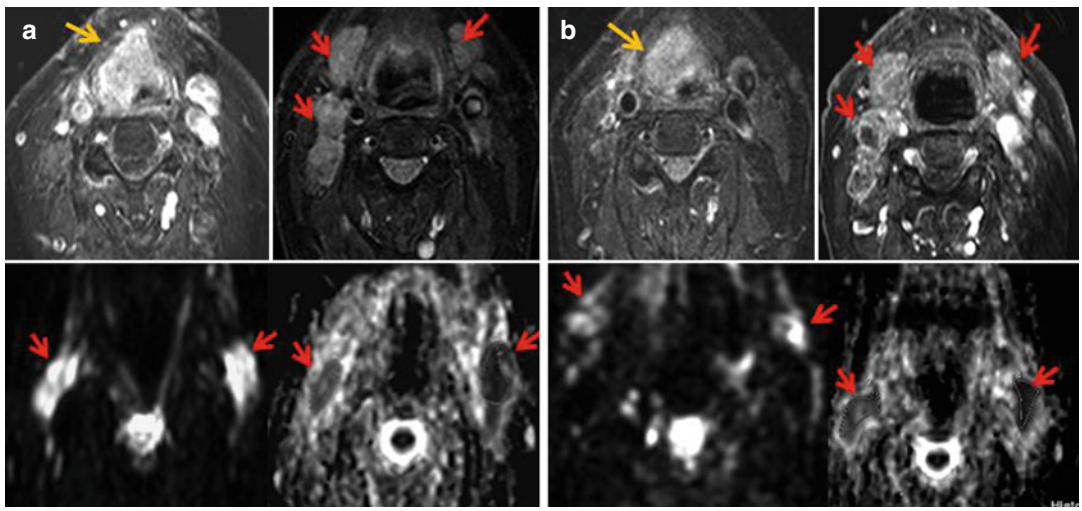

Fig. 28.9 Undifferentiated cancer of larynx with bilateral adenopathies. (**a**) Pretreatment MR exam demonstrates an enhancing and expansive lesion in the anterior and right aspects of the larynx (*yellow arrow*), associated to bilateral lymphadenopathies (*red arrows on right top image*), which show high signal on high *b* value and are hypointense on ADC maps (*red arrows on bottom images*). This behaviour is related to important diffusion restriction and high cellular density. (**b**) After the first cycle of chemotherapy, a partial response can be observed characterized by a decrease in tumor size and enhancement (*yellow arrow*). A reduction in lymph node size and heterogeneous enhancement (*red arrows in right top image*) are also noted, as well as a decrease of signal intensity on high *b* value diffusion-weighted image and an increase of ADC values (*red arrows in bottom images*), secondary to cellularity reduction indicating response to treatment

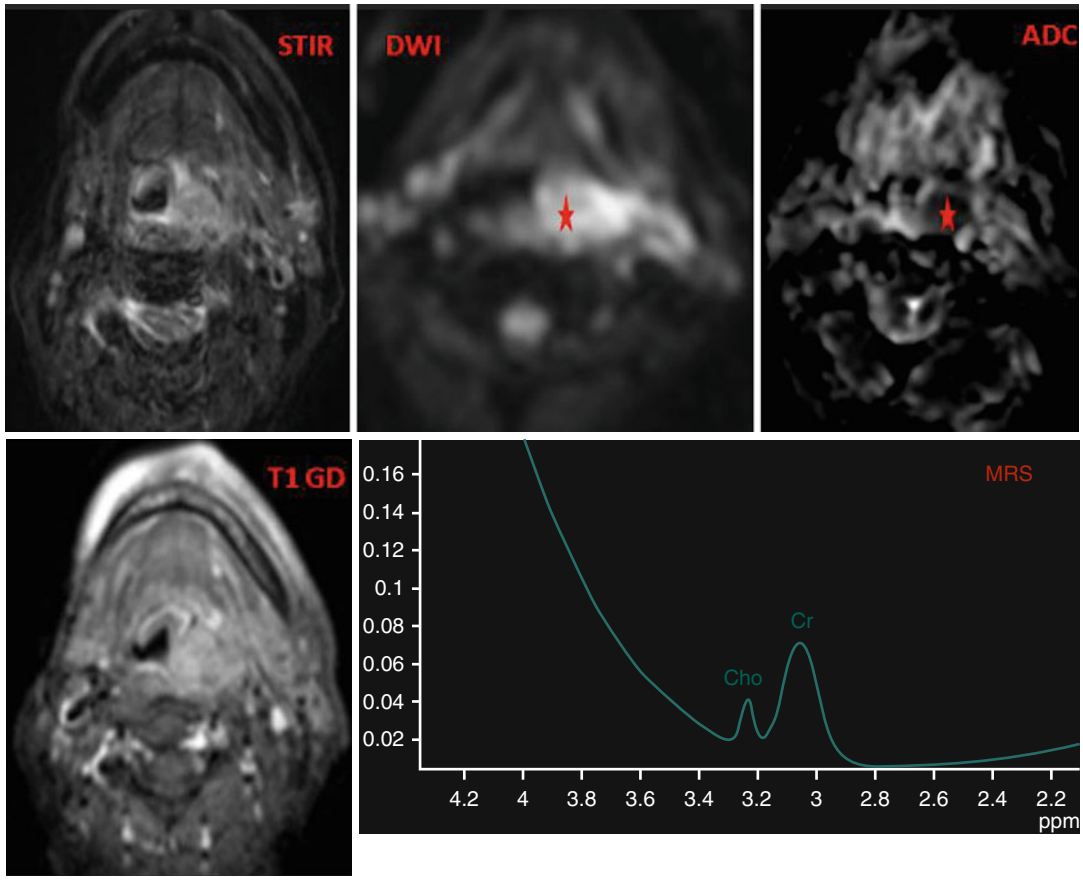

Fig. 28.10 Laryngeal cancer in situ treated 3 years ago. New metachronous oropharyngeal tumor. The lesion demonstrated high signal on STIR, enhancement on postcontrast fat-suppressed TSE T1-weighted image, restricted diffusion on DWI and low ADC value (*) of 0.82 x 10^{-3} mm^2/s. MRS shows a high peak of choline (Cho), which favours a malignant origin

has demonstrated less false-positive results than FDG-PET/CT in establishing recurrence, so DWI is described like a potential important tool for monitoring response in patients treated with chemoradiation and, furthermore, it could be very useful to predict outcome, and to differentiate responders from nonresponders earlier than other imaging techniques. For this purpose, ADC quantification may be useful for the analysis of the heterogeneity of tumors and their changes during treatment, thus being optimal to obtain evolutionary histograms or parametric response maps [25, 27, 73, 74].

Regarding MRS (Fig. 28.10), when choline is present in the posttreatment scenario, it is indicative of recurrence or residual tumor with a positive predictive value of 100 %. However, when choline is absent, there is a lower negative predictive value (81 %). In addition, MRS may be used in therapy montoring of HN cancer after treatment. The percentage change in Cho/Cr in a posttreatment mass after chemoradiotheraphy is correlated with residual cancer [75].

Multiple studies have demonstrated the superiority of PET over CDI for the identification of local or regional recurrence after treatment [73, 74, 76]. In a meta-analysis by our group in 2008, the utility of ^{18}F-FDG-PET in patients with suspected recurrence of HN tumors, the overall sensitivity in the 19 included studies was 94 % (95 % CI, 91–96), and overall specificity was

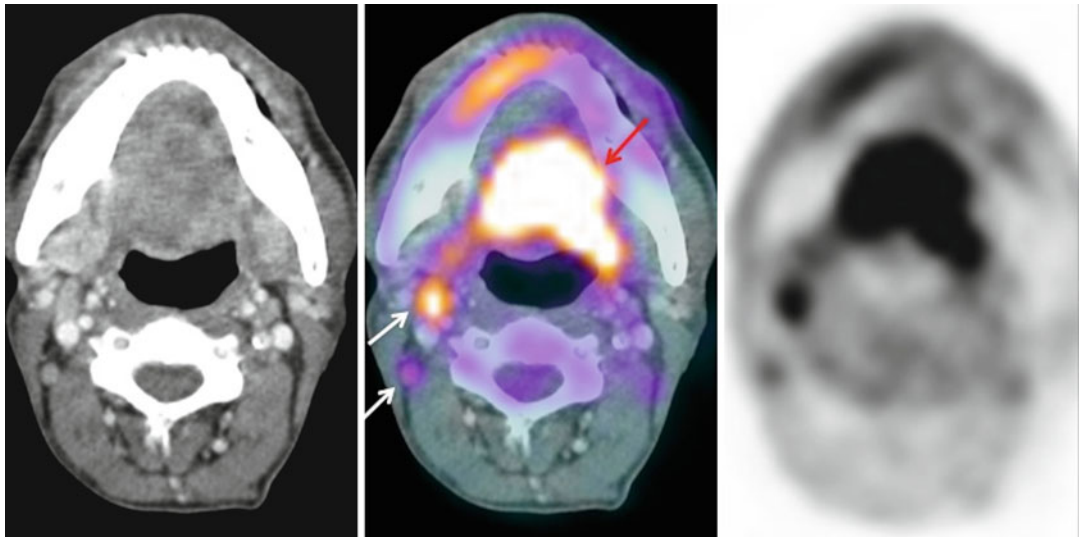

Fig. 28.11 52-year-old man with lingual squamous cell carcinoma treated with favourable chemotherapy. Appearance of indurated right tongue base lesion without evidence of malignancy in the biopsy. ^{18}F-FDG-PET/CT showed pathologic uptake in the tongue (*red arrow*) and in bilateral cervical adenopathies (*white arrows*). Biopsy confirmed poorly differentiated squamous cell carcinoma. He underwent traqueotomy, glossectomy with flap reconstruction and bilateral functional neck dissection. Chemotherapy was then administered

80 % (95 % CI, 76–84) [77]. In the follow-up, numerous studies using PET or PET/CT found sensitivity between 90–100 % in the detection of recurrent disease (Fig. 28.11), with lower specificity values (63–94 %), due to nonspecific uptake in inflammatory tissue, especially in patients with advanced tumors, in which posttreatment complications, such as mucositis and radionecrosis, are more prevalent. About the periodicity of PET/CT in the follow-up of HN tumors after treatment, it is recommended every 6 months for the first 2 years and then annually for 3 years [78].

28.5 Pitfalls in PET

Variable ^{18}F-FDG uptake in normal structures such as the nasal turbinates, pterygoid muscles, extraocular muscles, parotid and submandibular glands, and lymphoid tissue may confound interpretation and result in false-positive findings. Similarly, ^{18}F-FDG uptake in contracted muscles may lead to false-positive results. Localization of a lesion within or in proximity to an anatomic structure with high physiological ^{18}F-FDG uptake such as the brain or tonsils may make it difficult to assess pathologic uptake. In small lesions, the ^{18}F-FDG uptake may be underestimated owing to partial volume averaging with adjacent normal tissue. PET/CT performed within 3 months of radiation therapy may still yield false-positive or false-negative findings. Benign conditions, such as inflammation, infection, fistulas (Fig. 28.12), and granulomatous processes, may also demonstrate ^{18}F-FDG uptake. Tumors with inherently low FDG uptake such as salivary gland neoplasms and necrotic neoplasms may also yield false-negative results [79].

28.6 Summary

CT or MRI is of unquestionable utility in pretherapy staging and treatment monitoring in patients with HN tumors. However, morphologic imaging techniques are often inadequate to characterize HN lesions or discriminate small recurrences from others non-tumoral conditions, like vascularized scar tissue. In these cases, CT or MRI benefits of the integration with functional imaging techniques, such as perfusion CT, DCE-MRI, and DWI. ^{18}F-FDG-PET/CT offers valuable opportunities for the assessment of HN cancer in all phases of the disease. However, the

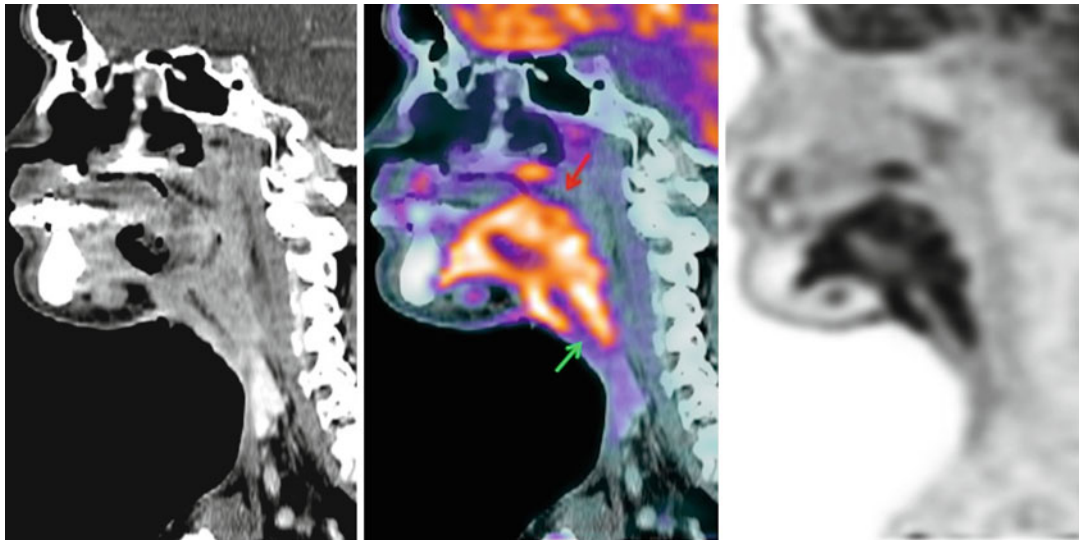

Fig. 28.12 A 48-year-old man with supraglottic carcinoma treated with pharyngolaryngectomy and chemoradiotherapy. ^{18}F-FDG-PET/CT performed to assess treatment response, suggested malignancy in an ulcerative lesion located on the floor of the mouth (*red arrow*), with adjacent linear ^{18}F-FDG uptake (*green arrow*), regarding postoperative complication (pharyngostoma). These findings were confirmed by histopathology

role of alternative tracers has still to be determined. This is in turn, one of the many exciting challenges that still lie ahead in a field in which it is crucial to go on setting our sights high [80, 81].

References

1. Stokkel MPM, et al. Preoperative evaluation of patients with primary head and neck cancer using dual-head ^{18}Fluorodeoxyglucose positron emission tomography. Ann Surg. 2000;231:229–34.
2. Curtin HD, et al. Comparison of CT and MR imaging in staging of neck metastases. Radiology. 1998;207:123–30.
3. King AD, et al. Comparison of CT and MR imaging for the detection of extranodal neoplastic spread in metastatic neck nodes. Eur J Radiol. 2004;52:264–70.
4. Takes RP, et al. The value of ultrasound with ultrasound-guided fine-needle aspiration biopsy compared to computed tomography in the detection of regional metastases in the clinically negative neck. Int J Radiat Oncol Biol Phys. 1998;40:1027–32.
5. Van den Brekel MWM, et al. Modern imaging techniques and ultrasound-guided aspiration cytology for the assessment of neck node metastases: a prospective study. Eur Arch Otorhinolaryngol. 1993;250:11–7.
6. Carmeci C, et al. Ultrasound-guided fine-needle aspiration biopsy of thyroid masses. Thyroid. 1998;8:283–9.
7. Schmidt RL, et al. A systematic review and meta-analysis of the diagnostic accuracy of ultrasound-guided core needle biopsy for salivary gland lesions. Am J Clin Pathol. 2011;136:516–26.
8. Grégorie V, et al. Squamous cell carcinoma of the head and neck: EHNS-ESMO-ESTRO clinical practice guidelines for diagnosis, treatment and follow-up. Ann Oncol. 2010;21:184–6.
9. Hermans R, et al. Imaging techniques. In: Head and neck cancer imaging. Berlin/Heidelberg: Springer; 2012. p. 33–54.
10. Franca C, et al. Use of three-dimensional spiral computed tomography imaging for staging and surgical planning of head and neck cancer. J Digit Imaging. 2000;13:24–32.
11. Magnano M, et al. Virtual endoscopy of laryngeal carcinoma: is it useful? Otolaryngol Head Neck Surg. 2005;132:776–82.
12. Ash L, et al. Head and neck squamous cell carcinoma: CT perfusion can help noninvasively predict intratumoral microvessel density. Radiology. 2009;251:422–8.
13. Surlan-Popovica K, et al. Changes in perfusion CT of advanced squamous cell carcinoma of the head and neck treated during the course of concomitant chemoradiotherapy. AJNR Am J Neuroradiol. 2010;31:570–5.
14. Sievers KW, et al. Paranasal sinuses and nasopharynx CT and MRI. Eur J Radiol. 2000;33:185–202.
15. Miles KA. Tumour angiogenesis and its relation to contract enhancement on computed tomography: a review. Eur J Radiol. 1999;30:198–205.
16. Kupisz K, et al. Tumor angiogenesis in patients with laryngeal cancer. Eur Arch Otorhinolaryngol. 1999;256:303–5.

17. Lentsch EJ, et al. Microvessel density in head and neck squamous cell carcinoma primary tumors and its correlation with clinical staging parameters. Laryngoscope. 2006;116:397–400.
18. Cao Y, et al. Early prediction of outcome in advanced head-and-neck cancer based on tumor blood volume alterations during therapy: a prospective study. Int J Radiat Oncol Biol Phys. 2008;72:1287–90.
19. Hoskin PJ, et al. Dynamic contrast enhanced magnetic resonance scanning as a predictor of response to accelerated radiotherapy for advanced head and neck cancer. Br J Radiol. 1999;72:1093–8.
20. Golay X, et al. Perfusion imaging using arterial spin labeling. Top Magn Reson Imaging. 2004;15: 10–27.
21. Pollock JM, et al. Arterial spin labeled MRI perfusion imaging: clinical applications. Magn Reson Imaging Clin N Am. 2009;17:315–38.
22. Schmitt P, et al. Quantitative tissue perfusion measurements in head and neck carcinoma patients before and during radiation therapy with non-invasive MR imaging spin-labeling technique. Radiother Oncol. 2003;67:27–34.
23. Hompland T, et al. Interstitial fluid pressure and associated lymph node metastasis revealed in tumors by dynamic contrast-enhanced MRI. Cancer Res. 2012;72:4899–908.
24. Loeffelbein DJ, et al. PET-MRI fusion in head-and neck oncology: current status and implications for hybrid PET/MRI. J Oral Maxillofac Surg. 2012;70: 473–83.
25. Chawla S, et al. Diffusion-weighted imaging in head and neck cancers. Future Oncol. 2009;5:959–75.
26. Padhani AR, et al. Diffusion-weighted magnetic resonance imaging as a cancer biomarker: consensus and recommendations. Neoplasia. 2009;11:102–25.
27. Thoeny HC, et al. Diffusion-weighted MR imaging in head and neck. Radiology. 2012;263:19–32.
28. Le Bihan D, et al. Separation of diffusion and perfusion in intravoxel incoherent motion MR imaging. Radiology. 1998;168:497–505.
29. Lu Y, et al. Extension of the intravoxel incoherent motion model to non-gaussian diffusion in head and neck cancer. J Magn Reson Imaging. 2012;36: 1088–96.
30. Sumi M, Nakamura T. Head and neck tumors: assessment o perfusion-related parameters and diffusion coefficients based on the intravoxel incoherent motion model. AJNR Am J Neuroradiol. 2013;34: 410–6.
31. Fong D, et al. Diagnostic accuracy of diffusion-weighted MR imaging for nasopharyngeal carcinoma, head and neck lymphoma and squamous cell carcinoma at the primary site. Oral Oncol. 2010;46: 603–6.
32. Hermans R. Diffusion-weighted MRI in head and neck cancer. Curr Opin Otolaryngol Head Neck Surg. 2010;18(2):72–8.
33. Herneth AM, et al. Diffusion weighted imaging: lymph nodes. Eur J Radiol. 2010;76:398–406.
34. Kim JK, et al. Feasibility of diffusion-weighted imaging in the differentiation of metastatic from nonmetastatic lymph nodes: early experience. J Magn Reson Imaging. 2008;28:714–9.
35. King AD, et al. Malignant cervical lymphadenopathy: diagnostic accuracy of diffusion-weighted MR imaging. Radiology. 2007;245:806–13.
36. Kwee TC, et al. ADC measurements of lymph nodes: inter- and intra-observer reproducibility study and an overview of the literature. Eur J Radiol. 2010;75:215–20.
37. Sumi M, et al. Discrimination of cervical lymph modes with diffusion-weighted MR imaging in patients with head and neck cancer. AJNR Am J Neuroradiol. 2003;24:1627–34.
38. Wang J, et al. Head and neck lesions: characterization with diffusion-weighted echo planar MR imaging. Radiology. 2001;220:621–30.
39. Eida S, et al. Apparent diffusion coefficient mapping of salivary gland tumors: prediction of the benignancy and malignancy. AJNR Am J Neuroradiol. 2007;28: 116–21.
40. Razek A, et al. Characterization of pediatric head and neck masses with diffusion-weighted MR imaging. Eur Radiol. 2009;19:201–8.
41. Akter M, et al. Diffusion tensor tractography in the head-and-neck region using a clinical 3-T MR scanner. Acad Radiol. 2009;16:858–65.
42. Son PM, Curtin HD. Head and neck imaging, chapter 45. 5th ed. St. Louis: Mosby; 2011. ISBN 978-0-323-05355-6.
43. Tse GM, et al. Correlation of biomarkers in head and neck squamous cell carcinoma. Otolaryngol Head Neck Surg. 2010;143:795–800.
44. Rijpkema M, et al. Effects of breathing a hyperoxic hypercapnic gas mixture on blood oxygenation and vascularity of head-and-neck tumors as measured by magnetic resonance imaging. Int J Radiat Oncol Biol Phys. 2002;53:1185–91.
45. Curvo-Semedo L, et al. USPIO-enhanced magnetic resonance imaging for nodal with head and neck cancer. J Magn Reson Imaging. 2006;24(1): 123–31.
46. Ng SH, et al. ^{18}F-FDG PET and CT/MRI in oral cavity squamous cell carcinoma: a prospective study of 124 patients with histologic correlation. J Nucl Med. 2005;46:1136–43.
47. Roh JL, et al. Utility of 2-[^{18}F]fluoro-2-deoxy-D-glucose positron emission tomography and positron emission tomography/computed tomography imaging in the preoperative staging of head and neck squamous cell carcinoma. Oral Oncol. 2007;43:887–93.
48. Veit-Haibach P, et al. TNM staging with FDG-PET/CT in patients with primary head and neck cancer. Eur J Nucl Med Mol Imaging. 2007;34:1953–62.
49. Mak D, et al. Role of FDG-PET/CT in staging and follow-up of head and neck squamous cell carcinoma. Q J Nucl Med Mol Imaging. 2011;55:487–99.
50. Platzek I, et al. PET/MRI in head and neck cancer: initial experience. Eur J Nucl Med Mol Imaging. 2012;40(1):6–11.

51. de Bondt RB, et al. Detection of lymph node metastases in head and neck cancer: a meta-analysis comparing US, USgFNAC, CT and MR imaging. Eur J Radiol. 2007;64:266–72.
52. Schöder H, Yeung HW. Positron emission imaging of head and neck cancer, including thyroid carcinoma. Semin Nucl Med. 2004;34:180–97.
53. Iyer NG, et al. Role of pretreatment ^{18}FDG-PET/CT in surgical decision-making for head and neck cancers. Head Neck. 2010;32:1202–8.
54. Murakami R, et al. Impact of FDG-PET/CT imaging on nodal staging for head-and-neck squamous cell carcinoma. Int J Radiat Oncol Biol Phys. 2007;68: 377–82.
55. Jeong HS, et al. Use of integrated ^{18}F-FDG PET/CT to improve the accuracy of initial cervical nodal evaluation in patients with head and neck squamous cell carcinoma. Head Neck. 2007;29:203–10.
56. Kyzas PA, et al. ^{18}F-fluorodeoxyglucose positron emission tomography to evaluate cervical node metastases in patients with head and neck squamous cell carcinoma: a meta-analysis. J Natl Cancer Inst. 2008;100:712–20.
57. Rodrigues RS, et al. Comparison of whole-body FDG-PET/CT, dedicated high resolution head and neck FDG-PET/CT, and contrast-enhanced CT in preoperative staging of clinically M0 squamous cell carcinoma of the head and neck. J Nucl Med. 2009;50: 1205–13.
58. Prestwich RJ, et al. The impact of 18F-FDG PET CT prior to chemoradiotherapy for stage III/IV head and neck squamous cell carcinoma. ISRN Oncol. 2012.
59. Prestwich RJ, et al. Delayed response assessment with FDG-PET-CT following (chemo)radiotherapy for locally advanced head and neck squamous cell carcinoma. Clin Radiol. 2012;67:966–75.
60. Yamazaki Y, et al. Assessment of cervical lymph node metastases using FDG-PET in patients with head and neck cancer. Ann Nucl Med. 2008;22:177–84.
61. Brouwer J, et al. Screening for distant metastases in patients with head and neck cancer: is there a role for (18)FDG-PET? Oral Oncol. 2006;42:275–80.
62. Ng SH, et al. Distant metastases and synchronous second primary tumors in patients with newly diagnosed oropharyngeal and hypopharyngeal carcinomas: evaluation of ^{18}F-FDG PET and extended-field multidetector row CT. Neuroradiology. 2008;50:969–79.
63. Lonneaux M, et al. Positron emission tomography with [^{18}F]fluorodeoxyglucose improves staging and patient management in patients with head and neck squamous cell carcinoma: a multicenter prospective study. J Clin Oncol. 2010;28:1190–5.
64. Brun E, et al. FDG PET studies during treatment: prediction of therapy outcome in head and neck squamous cell carcinoma. Head Neck. 2002;24:127–35.
65. Schöder H, et al. PET monitoring of therapy response in head and neck squamous cell carcinoma. J Nucl Med. 2009;50:74S–88.
66. Isles MG, et al. A systematic review and meta-analysis of the role of positron emission tomography in the follow up of head and neck squamous cell carcinoma following radiotherapy or chemoradiotherapy. Clin Otolaryngol. 2008;33:210–22.
67. Ong SC, et al. Clinical utility of ^{18}F-FDG PET/CT in assessing the neck after concurrent chemoradiotherapy for locoregional advanced head and neck cancer. J Nucl Med. 2008;49:532–40.
68. Porceddu SV, et al. Utility of positron emission tomography for the detection of disease in residual neck nodes after (chemo)radiotherapy in head and neck cancer. Head Neck. 2005;27:175–81.
69. Yao M, et al. The role of FDG PET in management of neck metastasis from head-and-neck cancer after definitive radiation treatment. Int J Radiat Oncol Biol Phys. 2005;63:991–9.
70. Rabalais A, et al. A cost-effectiveness analysis of positron emission tomography-computed tomography surveillance versus up-front neck dissection for management of the neck for N2 disease after chemoradiotherapy. Laryngoscope. 2012;122:311–4.
71. Chung MK, et al. Metabolic tumor volume of [^{18}F]-fluorodeoxyglucose positron emission tomography/computed tomography predicts short-term outcome to radiotherapy with or without chemotherapy in pharyngeal cancer. Clin Cancer Res. 2009;15:5861–8.
72. Takahashi T, et al. MRI perfusion study in head and neck cancers for early prediction of response to radiotherapy: a preliminary study. Aust-Asian J Cancer. 2006;5:219–23.
73. Chung W, et al. A prospective study of PET-FDG imaging for the assessment of head and neck squamous cell carcinoma. Clin Otolaryngol Allied Sci. 1997;22:209–14.
74. Kubota K, et al. FDG-PET delayed imaging for the detection of head and neck cancer recurrence after radio-chemotherapy: comparison with MRI/CT. Eur J Nucl Med Mol Imaging. 2004;31:590–5.
75. Abdel Razek AA, Poptani H. MR spectroscopy of head and neck cancer. Eur J Radiol. 2013;82:982–9.
76. Fischbein NJ, et al. Clinical utility of positron emission tomography with ^{18}F-fluorodeoxyglucose in detecting residual/recurrent squamous cell carcinoma of the head and neck. AJNR Am J Neuroradiol. 1998;19:1189–96.
77. Pasamontes JA, et al. Revisión sistemática y metaanálisis de la eficacia diagnóstica de la PET ^{18}F-FDG en recurrencia tumoral de cánceres de cabeza y cuello. Acta Otorrinolaringol Esp. 2008;59:190–7.
78. Soriano AM, et al. Tumores de cabeza y cuello. In: Carreras JL, editor. Utilidad de la PET-TAC en oncología. Serie de monografías Real Academia Nacional de Medicina. Arán Ediciones, Madrid, Spain. S.L.; 2010. p. 109–27.
79. Fukui MB, et al. Combined PET-CT in the head and neck. Part 2. Diagnostic uses and pitfalls of oncologic imaging. Radiographics. 2005;25:913–30.
80. Garg MK, et al. The evolving role of positron emission tomography-computed tomography in organ-preserving treatment of head and neck cancer. Semin Nucl Med. 2012;42:320–7.
81. Hustinx R, Lucignani G. PET/CT in head and neck cancer: an update. Eur J Nucl Med Mol Imaging. 2010;37:645–51.